

Explainable embeddings with Distance Explainer

Christiaan Meijer

E. G. Patrick Bos

Netherlands eScience Center

Science Park 402 (Matrix THREE)

1098 XH Amsterdam

C.MEIJER@ESCIENCECENTER.NL

P.BOS@ESCIENCECENTER.NL

Editor: JMLR editor

Abstract

While eXplainable AI (XAI) has advanced significantly, few methods address interpretability in embedded vector spaces where dimensions represent complex abstractions. We introduce Distance Explainer, a novel method for generating local, post-hoc explanations of embedded spaces in machine learning models. Our approach adapts saliency-based techniques from RISE to explain the distance between two embedded data points by assigning attribution values through selective masking and distance-ranked mask filtering. We evaluate Distance Explainer on cross-modal embeddings (image-image and image-caption pairs) using established XAI metrics including Faithfulness, Sensitivity/Robustness, and Randomization. Experiments with ImageNet and CLIP models demonstrate that our method effectively identifies features contributing to similarity or dissimilarity between embedded data points while maintaining high robustness and consistency. We also explore how parameter tuning, particularly mask quantity and selection strategy, affects explanation quality. This work addresses a critical gap in XAI research and enhances transparency and trustworthiness in deep learning applications utilizing embedded spaces.

Keywords: embedded spaces, explainable AI, attribution, multi-modal, saliency maps

1 Introduction

The soaring popularity in the last decade of machine learning (ML) and deep learning (DL) methods resulted in a high demand for understanding trained models. The field specifically aiming to solve this, eXplainable AI (XAI), has therefore been vibrant. XAI algorithms are continuously developed for images, text, time-series and tabular data (Vilone and Longo, 2021). However, XAI methods for general “embedded spaces” are less common.

By the term “embedded space” we refer to a multi-dimensional vector space which original data can be projected or encoded into. “Latent space” is a popular alternative term. Embedded spaces are used in dimensional reduction operations that aim to preserve certain properties of the original data, for instance in applications like FaceNet (Schroff et al., 2015), Word2vec (Church, 2017), VAE (Kingma and Welling, 2019), Spec2vec (Huber et al., 2021), and Life2Vec (Savcisens et al., 2024). Multi-modal models such as CLIP (Radford et al., 2021) project multiple data modalities into shared embedded spaces. The

©2025 Meijer and Bos.

License: CC-BY 4.0, see <https://creativecommons.org/licenses/by/4.0/>. Attribution requirements are provided at <http://jmlr.org/papers/v1/00-000.html>.

increasingly broad scientific application of (multi-modal) embedded space models to model complex phenomena, e.g. for studying visually grounded language learning (Chrupala, 2022) to learn about analogies with human learning, make explainable methods especially promising and urgent for increasing the efficiency and trustworthiness of research far beyond the domain of AI research itself (see also e.g. Yang et al., 2022; Gade et al., 2019; Gevaert, 2022).

The structure of embedded spaces created by methods such as deep neural nets are by nature difficult to understand as its dimensions often represent multi-step abstractions of the original data space (Shahroudnejad, 2021; Bau et al., 2020). Nevertheless, the structure of some embedded spaces can be made more interpretable using XAI methods (Ali et al., 2023; Boselli et al., 2024). A variety of XAI methods have been developed to interpret and explain model predictions, and these can be broadly categorized based on their approach. Much of the work done for embedded spaces specifically has been focused on the *interpretability*¹ of the spaces or the model as a whole (Boselli et al., 2024). Methods for interpretability can be contrasted with methods for *explainability* of model decisions. To the best of our knowledge, no methods are currently available for explaining individual model decisions for embedded vectors.

In particular, the method introduced in this paper provides a local, post-hoc explanation of aspects of distance between two data items’ projections within embedded spaces. In general, quantifying the input’s features’ effect on the model output is called attribution (Achtibat et al., 2023). Other local, post-hoc methods like RISE (Petsiuk et al., 2018), LIME (Ribeiro et al., 2016) and GradCAM (Selvaraju et al., 2020) take a single input data instance, and calculate the effect of its features on the output of the model that is being explained. Our method however, processes a single data instance by comparing to some other reference data instance.

In this paper we introduce a method to locally explain embedded spaces using attribution. In section 2 we describe the what and why of our method. In the rest of the paper, we evaluate its performance. To do so, we ran experiments on a set of models and data items that we list in section 3. We assess the results of the experiments on our explainer using proven quantitative measures in section 4. We also test the explainer’s usefulness from our own human point of view in the intuitive qualitative assessment of section 5. Open questions, future work and other concluding remarks are provided in sections 6 and section 7.

2 Algorithm

We consider a model that encodes data instances from multiple data modalities into an single vector space. For example, the CLIP model encodes both image data and text data into a common semantic vector space, making it possible to reason about semantic similarity between instances from different modalities. Proximity between instances in this space can be interpreted as semantic similarity. We would like to be able to ask the model

1. We follow the XAI nomenclature proposed by (Ali et al., 2023).

why certain instances end up closer to each other than others. This question is what our proposed algorithm is developed to address.

2.1 Algorithm description

Our starting point was RISE (Petsiuk et al., 2018), a method that assigns saliency values to each pixel or region of the input data. It does so by randomly masking pixels in a given image and examining the effect on the model’s activation value of a user-specified class of interest. Reasons for choosing RISE include that an implementation was freely available, that it is easy to reason about and hence to extend. Also, RISE is model-agnostic; it does not need any internal information about the model, making it widely applicable. Finally, by masking randomly, the method feeds into the model different parts that potentially hold the most meaning when they’re combined, as opposed to masking isolated regions and ignoring the meaning of combinations of parts. This way, it is sensitive to a wide range of semantic contents.

Task The RISE implementation accompanying the original paper (Petsiuk et al., 2018) was tailored to the task of classification, specifically on images. In Rangelova et al. (2024), RISE was extended to classification on tabular data, textual data and time series. In this work, we extended the method to a task that differs in 2 important aspects:

1. In our task, both input and output types are different to what is the case in a classification task. The classification task only has one input data-point, and the model is asked to output a certain class, or more generally a vector of activations over some class-space. In the current task, however, the model gets two input data-points and outputs a single distance of the two encoded inputs in the embedded space.
2. The RISE algorithm for producing the saliency map explaining a certain class equals a weighted sum over the randomly generated masks, where the weights are derived from the model’s output probability (or rather activation value) for the masked image (see Petsiuk et al., 2018, for more details, especially equation 6 therein). For our task, we do not have class probabilities. Instead, we have 2 points in an embedded space with an associated distance between them. As we will discuss below, converting this distance to a RISE weight was a crucial, non-trivial problem for us to solve.

The above considerations lead us to the following three modifications to the original RISE method.

1. Because we consider two input items, but only one output saliency map, we define one of the input items to be a “reference” item, and the other to be the “to-be-explained” item. This results in the advantage that the “reference” item can be input to the algorithm in encoded form (i.e. already encoded into embedded space by the model). Therefore, the algorithm implicitly supports any data modality of the reference item. For the data modality of “to-be-explained” item, however, support explicitly needs to be implemented including a sensible masking strategy and visualization.

2. The class-activation weight is replaced by the cosine distance $d_{\cos}(e, r)$ between the “to-be-explained” item e and the “reference” item r . However, we do not directly use $d_{\cos}(e, r)$ in the same way as in RISE, i.e. in a weighted sum over all masks. See Section 2.2 for discussion on this point.
3. We introduce a distance-ranked mask filtering method. We only sum over the masks that meet our filter criterion. Before filtering, the distances are used to rank the masks. Filtering then proceeds according to one of three methods:
 - (a) taking masks associated with the top $x\%$ of distances,
 - (b) the bottom $x\%$
 - (c) or combining these two sets, which we call the “mirror” approach.

The reasoning behind these three methods is as follows. For masked images where the distance to the original image is low, the masked pixels apparently did not contain much salient information. Hence, masks associated with them should contribute to (through the sum over masks) highlighting minimally salient regions. In contrast, masks associated with high distances contribute to highlighting maximally salient regions². Selecting from either side should give a distinction between highly and lowly salient regions. Combining both these sources (the “mirror” filtering method), assuming similar statistical properties and sizes of the both sets, an improvement of the signal to noise ratio could be expected in each pixel due to one side partially canceling out the noise of the other side (relative to the signal).

After filtering, the remaining masks are summed. In contrast to the original RISE method, we sum without multiplying by any weights (see Section 2.2 for motivation). In the “mirror” method, we subtract the masks from one set from the other, since they are expected to be “mirrors” in terms of their explanatory contents, as explained above.

2.2 Considered algorithm alternatives

2.2.1 DISTANCE METRIC

We chose a cosine distance $d_{\cos}(x, y)$ to compare points x and y in embedded space. Another obvious metric to use would have been the Euclidian distance. Because we use the distances, not to weigh, but just for ranking, the cosine distance is equivalent to the Euclidian distance (since one is proportional to the square of the other), in the special case that vectors are normalized to unit length beforehand. In the unnormalized case, however, cosine distance emphasizes angular differences between vectors while Euclidian distance emphasizes differences in vector length.

The first of the embedded spaces we applied our method on, an Imagenet classifier (see section 3.1 for more details on the model), is not normalized to unit vectors, but rather is a

2. One may note that these two maps can be expected to be very similar in appearance, although inverted in values, which is why we call them “mirrors” below.

list of activation values, sometimes interpreted as probabilities, where the elements sum to 1. Because Euclidian distance is dependent on vector size and these non-unit vectors can have sizes in the range of $[1/\sqrt{D}, 1]$, where D is vector dimension, Euclidian distance will have the unwanted effect of becoming smaller when the model is less certain of its classification, i.e. when activation values are distributed more broadly over dimensions (classes).

The second embedded space employed in this work is generated by the CLIP model, which does not hold this specific property. Therefore, in this case a different distance metric may be more suitable for certain applications. Exploring this is out of the scope of this work.

We emphasize that these are particularities of the models and layers of choice in this work. In general, the ideal distance metric is dependent on the properties of the particular embedded space.

2.2.2 RANKING OR WEIGHTING

Analogous to RISE, we initially experimented with weighting masks by a factor proportional to $d_{\cos}(e, r)$. However, we soon found that in the high dimensional embedded spaces of our applications differences between distances from one input item to the next were very small, typically below 10^{-4} . Weights based on these distances are very close together and hence do not distinguish the importance of one mask from another in a numerically significant way in the RISE algorithm. RISE was designed for weights in the range of $[0, 1]$. Our first attempt to solve this issue was to use a weight proportional to a^d , where d is distance and a is a value around 20. This blew up small numerical differences so that they would again form distinguishing weights. However, we found results lacking: to get sensible results (visually), we had to tune the a parameter for each new instance we wanted to explain. Moreover, in many cases, the end result was that a too small number of masked images would have high enough weights to have a significant effect on the resulting saliency map, leading to artifacts of the particular masking scheme to show up clearly in the result. This led us to our final approach, ensuring a fixed percentage of effective masks, hence avoiding masking artifacts.

2.3 Algorithm summary

We can now summarize the “Distance Explainer” algorithm. Given that we take RISE as the basis of our explanation method, and RISE works on only one data item, we run our explainer as follows:

1. The “reference” item r , is passed through the model to produce its position in embedded space \mathbf{x}_r . This position is then used as a fixed input to our explainer.
2. The following is repeated N_{masks} times on the “to-be-explained” item e :
 - (a) e is randomly masked according to the RISE masking algorithm (given a set of configuration parameters c , see Section 5.2) producing masked input item $M_i(e; c)$ at iteration i .

- (b) $M_i(e; c)$ is passed through the model to produce an embedded space position $\mathbf{x}_{M_i(e;c)}$.
 - (c) Distance $d_i = d_{\cos}(M_i(e; c), r)$ between \mathbf{x}_r and $\mathbf{x}_{M_i(e;c)}$ is calculated.
3. The distances $\{d_i\}$ for all masked input images are used to rank the masked images.
 4. A selection filter is applied on the ranked masked input images, as explained in Section 2.1.
 5. After filtering, the remaining masks are summed to produce the attribution map.

Our implementation of the algorithm is available on GitHub³.

3 Experimental setup

To experiment with the explainability of distances in embedded spaces, we need models that enable us to compare the position in embedded space of one data item to that of another item. In this section we describe the models and data items we use in our experiments to assess our explainer in sections 4 and 5.

A gallery of all experiment results applied on all item pairs is available on Zenodo⁴. The code used for the experiments is available on GitHub⁵.

3.1 Data item modalities and embedded space models

We have run our experiments on the following two pairs of data item modalities and associated models for transforming data items into a common embedded space:

Image vs image For this modality pair, we use ImageNet models to transform data items to a 1000-dimensional ImageNet classification vector. For each of the 1000 ImageNet classes, the corresponding vector element gives the activation of the model on that class. While this would not typically be considered an embedded space vector, it is structurally similar and can be interpreted as a kind of semantic vector in an albeit quite arbitrary but in fact also quite well defined space. This latter fact makes it especially suited for our experiments, as we can unequivocally interpret the “embedded space” vectors. In most experiments we used ResNet50 from Keras. In section 4.3 we used VGG16, because it has a smaller number of layers.

Image vs caption For this modality pair we did use an actual embedded space model, namely the ViT-B/32 (Dosovitskiy et al., 2021) CLIP model (Radford et al., 2021). It transforms both images and captions to a common 512-dimensional semantic vector space.

3. https://github.com/dianna-ai/distance_explainer

4. <https://zenodo.org/records/14044386>

5. https://github.com/dianna-ai/explainable_embedding/

In this work we restrict ourselves to attribution maps on images, so we only use the captions as reference items⁶.

3.2 Data items

For the Imagenet model, the data item pairs we used in our experiments were chosen to probe performance in four application areas of the algorithm:

Same class We explain the ImageNet model, using two images of the same class (e.g two different images of a bee). We expect highest attribution scores for the pixels of areas that we consider key aspects for the specific class.

Multiple classes per image Classification is slightly complicated by having multiple classes in one image. We use an image containing both a dog and a car and compare that to images containing only a dog or only a car.

Close and/or related classes We compare an image of a bee to an image of a fly. Here we expect to see the algorithm highlight the wings and general insect-like characteristics of the animals that contribute to their closeness, while the stripes that saliently distinguish a bee from a fly are given as reasons for greater distances.

Similarly, we compare an image of a car to that of a bike. Both may have similar traffic surroundings, and both have wheels, but the rest of the structure is quite different.

“Opposite” items (that have nothing in common) In this category we compare for instance a flower and a car.

A similar set of data pairs was explored for the CLIP model comparing images to captions:

Bee image - “a bee sitting on a flower” We expect the explainer to highlight both flower and bee.

Bee image - “a bee” Where we expect only to see the bee being highlighted.

Bee image - ‘an image of a bee’ Specifying the caption this way may improve performance for CLIP.

Bee image - “a fly” Close and related class. We expect elements of an image, depicting a bee, that are also present in images of flies, to be highlighted, while element that are not present in images of flies, not to be highlighted.

Bee image - “a flower” Can the other main object in our bee image also be detected or is a flower not salient enough for CLIP?

6. To do this in other data domains one needs to define a good masking function for that modality. In the DIANNA project (Rangelova et al., 2024), we have implemented masking for text, tables and time-series (Meijer, 2024).

Labradoodle image - “a labradoodle” Single salient object, simple caption.

Image of a dog and a car - “a car” and “a dog” Again the “multiple classes per image” case, compared to single object captions.

Flower image - “a car” An “opposite items” example.

Car image - “a bicycle” The “close and/or related classes” example.

4 Quantitative performance results

In this section we explore quantitative performance aspects of our explainer. Quantifying the quality of explanations is a field still much in motion. Nauta et al. (2023) provide an overview on how to evaluate various aspects of XAI methods. To assess Nauta’s Correctness and Completeness, we use the Incremental Deletion algorithm (van der Spek, 2023, p.27) and MPRT (Adebayo et al., 2020). To assess Continuity we use Average Sensitivity (Bhatt et al., 2021). Note that recent research (Hedström et al., 2024) provides robustness improvements in score calculation over the original MPRT method. However, we do not use the direct MPRT score output itself, because those are mainly useful for comparing multiple XAI algorithms, while we evaluate a single XAI algorithm. Instead, we qualitatively interpret the attribution maps from the intermediate steps in MPRT. The improvements in score calculation robustness the new methods – while we recommend using them when scoring itself is the goal – do not provide any added benefits for our purposes. For both MPRT and Average Sensitivity we used software implementations in Quantus (Hedström et al., 2023), adapted to work with our specific task as opposed to classification. For the chapter headers, we therefore use the Quantus terminology instead of Nauta’s. The methods we used, faithfulness, sensitivity/robustness and randomization align with Nauta’s concepts of Correctness, Continuity and Completeness, respectively.

4.1 Faithfulness

Explainers such as ours function by highlighting salient parts of input images (or data items more generally). The concept of faithfulness evaluates whether altering these highlighted regions produces corresponding changes in the model’s output—whether that output is a classification or, in our specific case, a distance measurement. In essence, *faithfulness* measures the extent to which an XAI method successfully identifies truly meaningful components of the input. A faithful explanation highlights precisely those elements that genuinely influence the model’s decision-making process.

We measured faithfulness of our explainer using the incremental deletion method. We ran it using three different deletion orders:

1. starting with pixels that contribute most to the two data items having a low distance; “LoDF” for low distance first,

2. starting with pixels that most contribute to high distance; “HiDF”⁷ for high distance first,
3. random order.

We illustrate and discuss the results from two image pairs: bee versus fly in figures 1 and 2 and bee versus another bee in figures 3 and 4. In Figure 2 and Figure 4 we see the respective “model scores” of these orders, in our case simply the resulting distance. LoDF and HiDF orders are shown in blue in separate panels, while random order is shown in both images in orange.

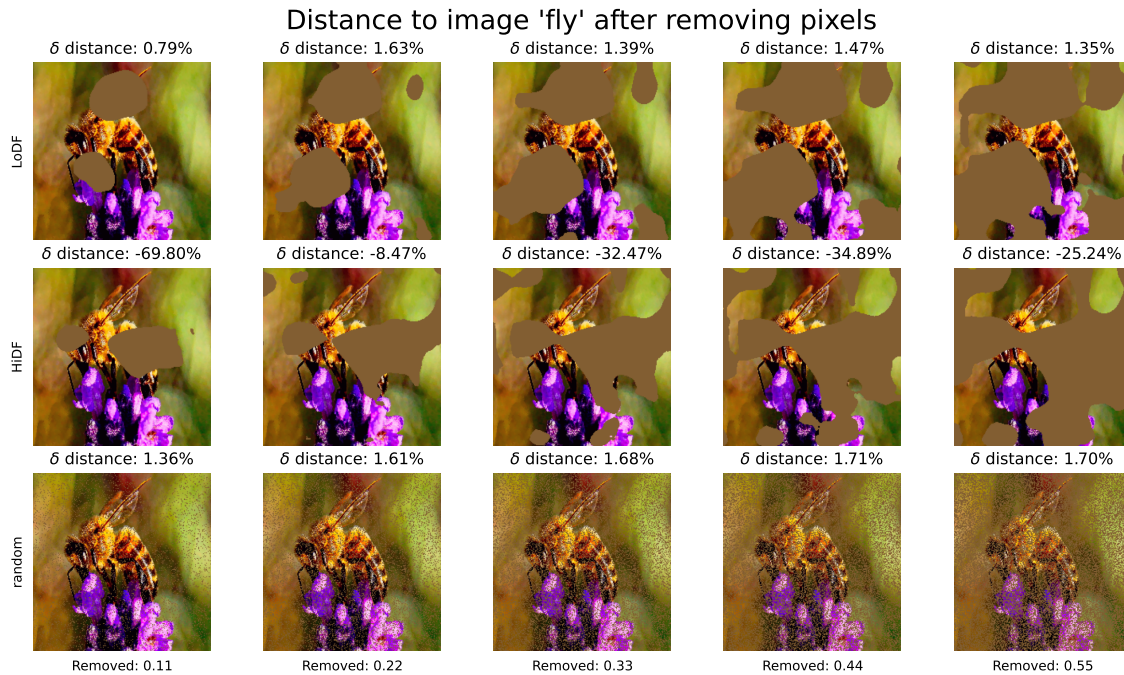


Figure 1: Incremental deletion on the bee image whose distance to a fly’s image is explained. Deleted pixels are coloured brown. From left to right, in every column a larger percentage of pixels is deleted. The top row has LoDF order. The middle row has HiDF order. The bottom row has random order.

7. We use the terms LoDF and HiDF instead of the “most/least relevant first” (MoRF/LeRF) terminology that is common in the literature on incremental deletion. We need different terms, for two reasons. First, because our maps are not “relevance” maps of pixels contributing to a certain classification (the task most often studied in this context) with some positive intensity, but are a bidirectional map of pixels that contribute either to an increase or a decrease of embedding vector distance, with a certain positive or negative intensity. Second, even if one would equate that intensity with relevance, one would have to deal with the fact that high positive and high negative intensity are two “modes” of “high relevance” that cannot be combined into one MoRF measure without losing critical information. On top of this, “LeRF” does not map straightforwardly to anything in our situation.

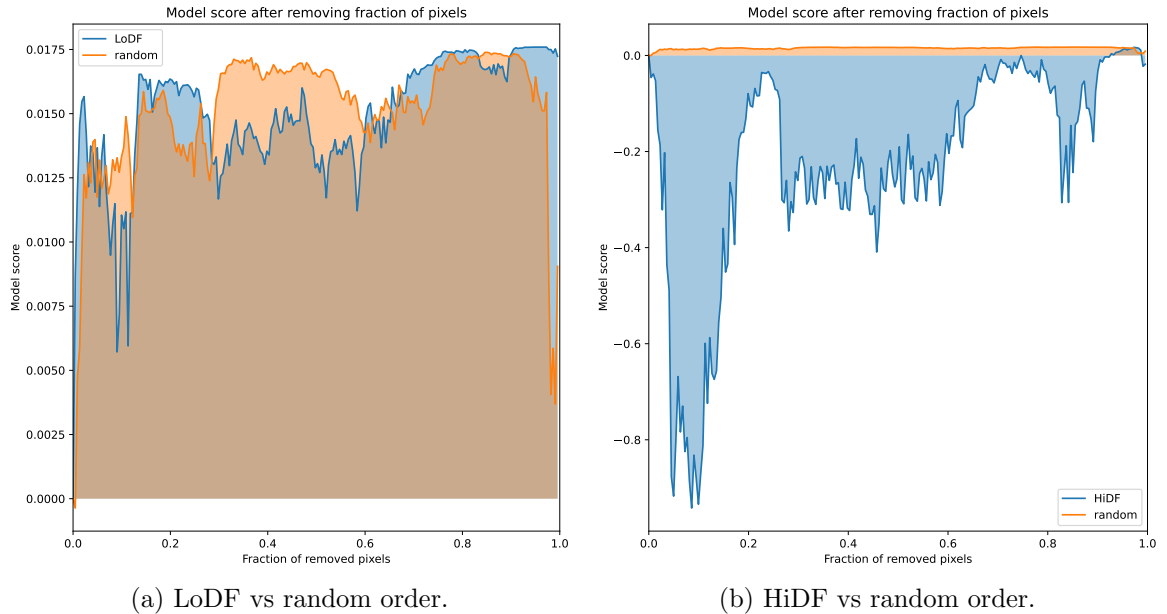


Figure 2: The vertical axis shows distance under incremental deletion on the bee image whose distance to a fly image is explained. Percentage of deleted pixels on the horizontal axis.

4.1.1 HOW TO INTERPRET THESE RESULTS?

The “bee versus fly” graph in figure 2b removes the least fly-like pixels first. These are pixels that are indicative of a bee and not of a fly. Removing them significantly changes the model’s class predictions. The model classifies the original image as a bee, so there is a lot of distance towards the fly classification part of the embedded space. Therefore, removing pixels in this order results in large changes in distance. This explains the large decrease (large negative values). Figure 2a shows results when removing most fly-like pixels first. These are parts of the image that look like they could be parts of a fly and hardly influence the model’s scores with respect to its scores towards the bee class. The reason is that the model was already predicting the images as a bee, and not a fly, with high confidence. There is almost nothing to gain here, and therefore any change in distance is small, comparable to random pixel removal.

The second experiment compares two bee images. Two results in particular caught our attention:

1. Why is the striped part of the bee (the posterior segment) not highlighted by the XAI method? Both in the LoDF and the HiDF panels of figure 3 it seems to be of limited relevance to the distance.
2. Why is the order of magnitude of the model scores so much higher in figure 4 than in figure 2?

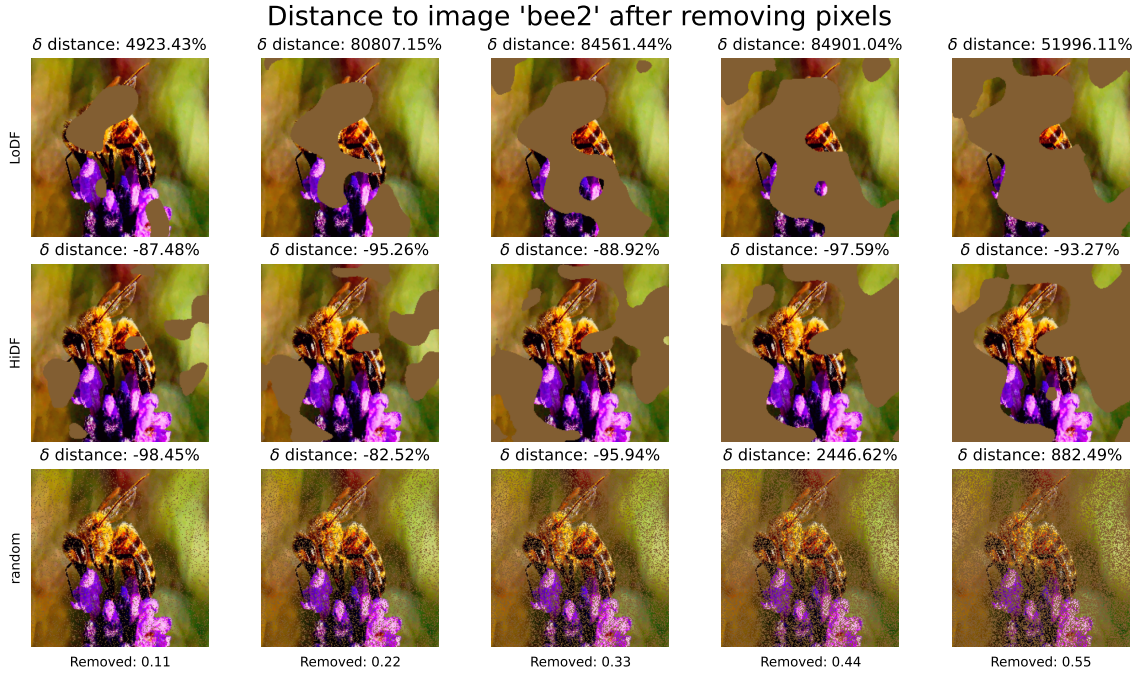


Figure 3: Incremental deletion on the bee image whose distance to *another bee's* image is explained. See the caption of figure 1 for a description of the rows and columns.

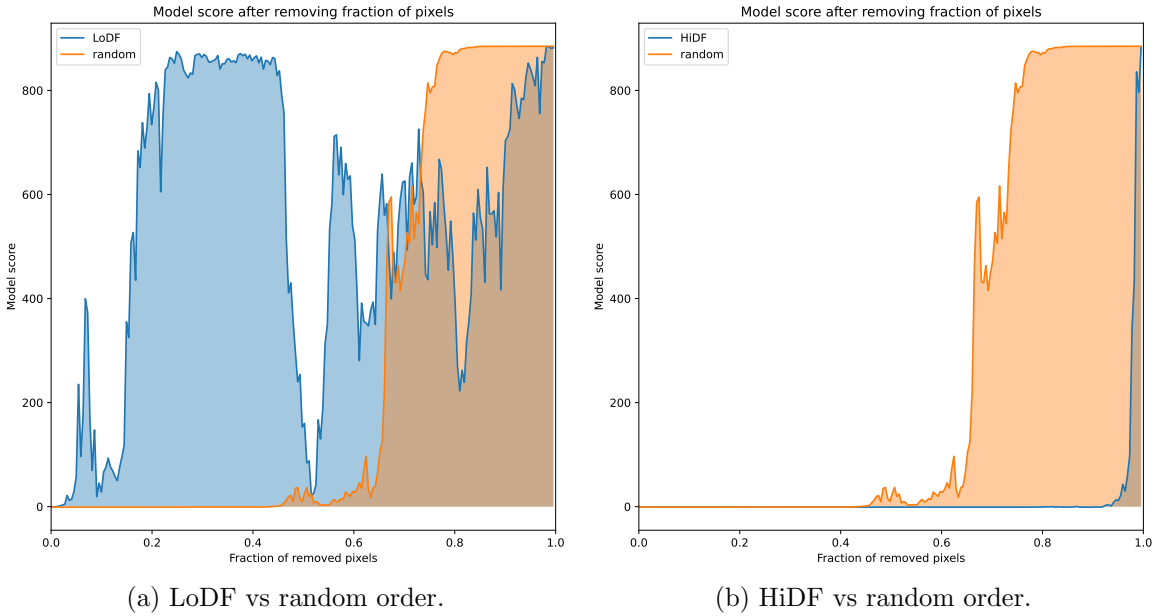


Figure 4: Like figure 2, but with another bee image as reference item.

The former seems due to the reference bee image having a lower contrast stripe pattern than the bee image shown here. In fact, this image is a painting of a bee, not a photograph. The artist may have exaggerated the stripe pattern compared to natural bee stripes.

The second question can be answered by considering the structure of the “embedded space”, namely the 1000-dimensional ImageNet classification vector. A pretty certain classification of a bee yields a vector that looks something like

$$(\text{class}_A, \dots, \text{bee}, \dots, \text{class}_Z) = (0.00001, \dots, 0.98, \dots, 0.00001), \quad (1)$$

which will have a very small distance to the other bee image’s vector. The maximum uncertainty classification vector, i.e. the vector representing equally likely classes, is

$$(\text{class}_A, \dots, \text{bee}, \dots, \text{class}_Z) = (0.001, \dots, 0.001, \dots, 0.001). \quad (2)$$

The distance between these two vectors is about 0.979. The *change* in distance from ~ 0 (one bee versus another bee) to 0.979 (one bee versus maximum uncertainty) is also ~ 0.979 . Looking at figure 4a, we see indeed the distance to the reference point increasing by removing the most bee-like parts. Starting from 15%, the distance increases almost maximally away from the bee, meaning that it is now classified as something other than a bee (perhaps a flower, in this case). Looking at the random order curve, not a lot happens while removing the first 55%, indicating that the image still scores highest in the bee dimensions. In other words, it still looks like a bee. This can be confirmed by looking at the last column in figure 3. The same happens in the HiDF order. Only the last 5% changes the model’s activations. Changes occur after removing more of the image than in the random order.

4.2 Sensitivity / robustness

Robustness refers to the property that small changes in the input should result in correspondingly small changes in the output. This ensures that the explainer’s results are stable and not overly sensitive to minor perturbations in the input data.

We use the Average Sensitivity metric (Bhatt et al., 2021) to measure the robustness of our explainer. The Quantus (Hedström et al., 2023) implementation we use, described in more detail in Yeh et al. (2019), has an expected value range typically between 0 and 1, sometimes above 1. This can be explained by the fact that the metric is based on a ratio of two quantities. The numerator is the difference in attribution values between two attribution arrays: one for the unperturbed input image and one for the perturbed image. The denominator is the unperturbed attribution array.

In these experiments we make MC sampling in the RISE-based part of our algorithm (the random mask generation) deterministic, otherwise we would have two sources of randomness when measuring robustness. We set Average Sensitivity parameters to `nr_samples = 20` and `perturb_std = 0.1 * 255`, i.e. 10 percent of the maximum range given by RGB integer images that in each channel run from 0 to 255. We use 500 masks.

We again focus here on the results of running this metric on the same two cases as for faithfulness: 1. the bee image versus the fly reference image case and 2. the bee versus

the other bee reference image case. The Average Sensitivity results are 0.06 for the “bee versus fly” case and 0.04 for the “bee versus bee” case. These are low sensitivity numbers, meaning the robustness of the explainer is high.

Note that a minor limitation in the Quantus implementation of Average Sensitivity is that lower and upper limits of resulting perturbed image values cannot be set. In principle, images should not contain values below 0 or above 255, but with a normally distributed noise function, such values will certainly occur occasionally, making the input data go out of distribution to some extent. We expect the effect of this to be minor.

4.3 Randomization

An XAI method should explain the model’s decisions. The result of running the XAI method should therefore be highly dependent on the model. This is tested using a *randomization* test, which assesses whether the explainer’s output changes as expected when model parameters are changed randomly.

We tested our XAI method using the Model Parameter Randomization Test (MPRT) (Adebayo et al., 2020) which is a popular randomization test (Hedström et al., 2024). MPRT randomly perturbs the weights in each model layer by shuffling them. The MPRT implementation in Quantus offers 3 modes: incrementally shuffling layers top-down, incrementally bottom-up and shuffling each layer independently. After perturbing the layers, MPRT summarizes its assessment in a metric: the Spearman correlation between the original “unperturbed” attribution map (i.e. without random perturbation of model layers) and the attribution map of a model with one or more randomized layers. The progression of this value from 1 (i.e. the unperturbed map’s correlation with the first “perturbed” map with zero perturbed layers) to something less than one can be used to characterize the explainer (although see the discussion in the introduction paragraph of this section about more robust characterization).

In table 1 the MPRT scores are shown for each layer, and for each of the 3 “modes”. For both top-down and bottom-up modes, correlations with the original attribution map are low after randomizing the first layer already, indicating a high dependency of the attribution map on the model. The independent mode shows high correlations for certain layers. This is puzzling given the low correlation scores of the first 2 modes. Possibly these particular layers have low variance in their weights and shuffling them only has a small effect on the model’s output.

In addition to the quantitative metric, we inspected the resulting attribution maps⁸ of the distance explainer while tested through all 3 modes. For input data we use an image of a bee, and a reference point of an image of a fly. We use `n_masks=1000`. Results are shown in Figures 5, 6 and 7.

8. The Quantus implemenation does not itself return these maps. Rather, they are used as intermediate results. To be able to inspect them, we modified the code so that the maps would be stored after each MPRT run.

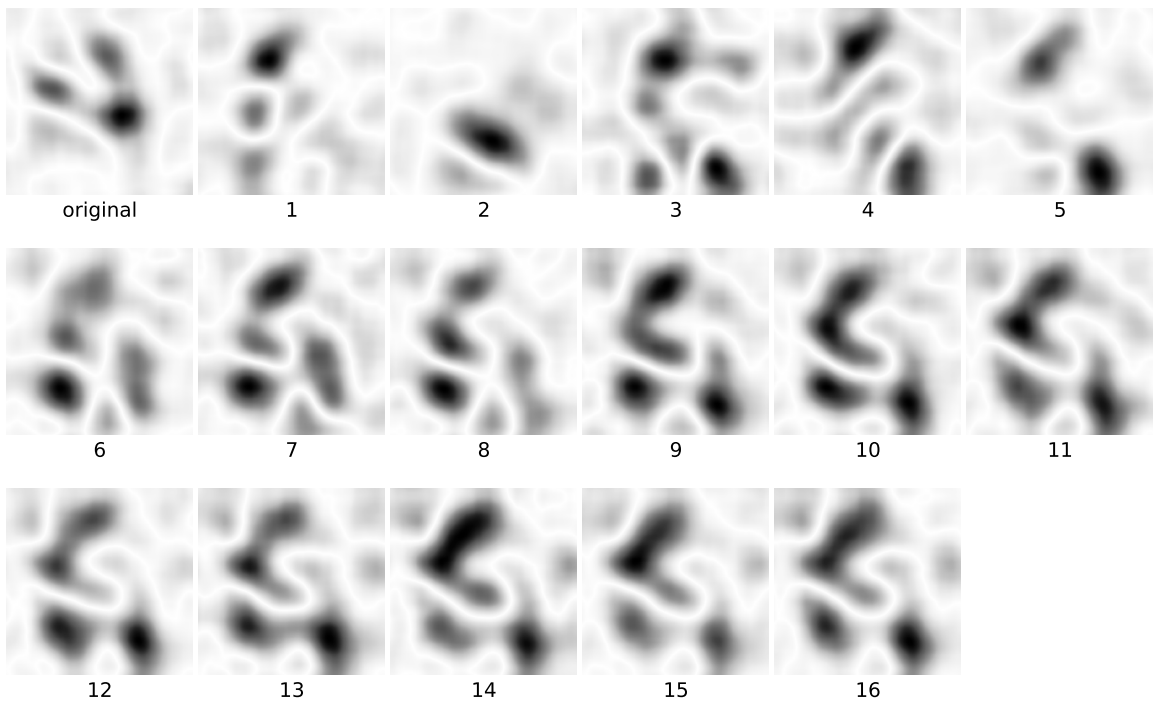


Figure 5: MPRT (top-down) results: The first image shows the saliency map for the unperturbed model. From left to right, the second images onwards show saliency maps for the model of which iteratively one additional layer has its weights perturbed, starting with the final fully connected layer and ending with weights of all layers in the model perturbed.

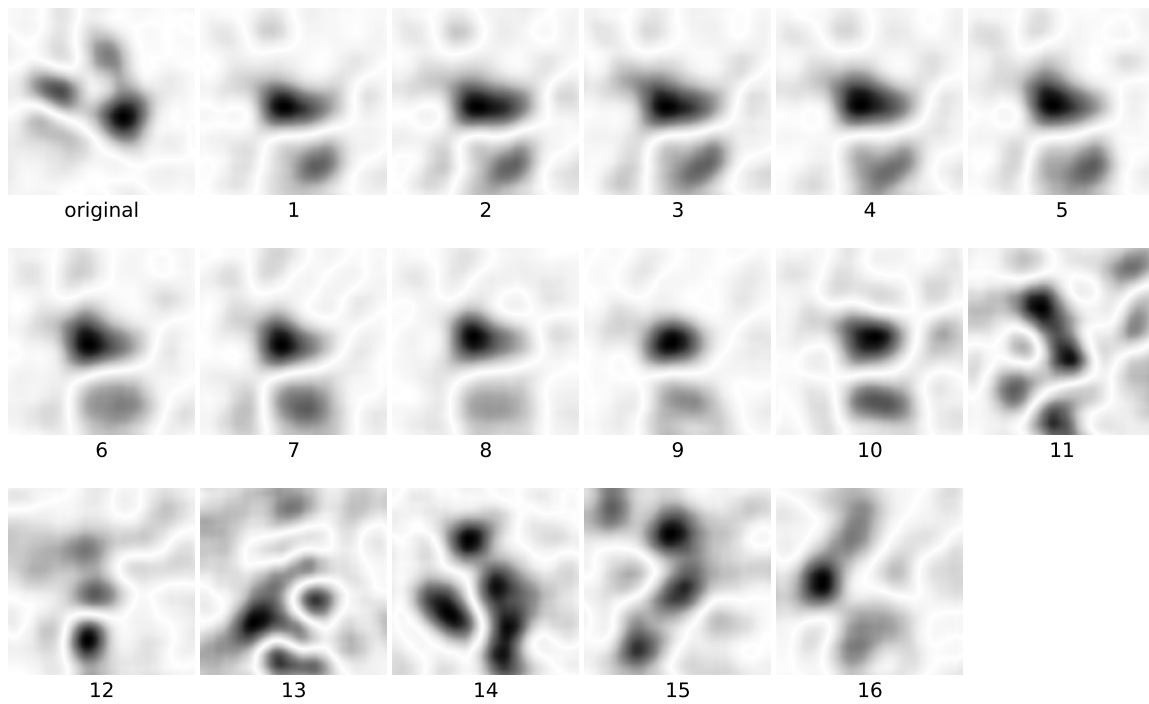


Figure 6: MPRT (bottom-up) results. Like figure 5, except here perturbation starts with the first layer.

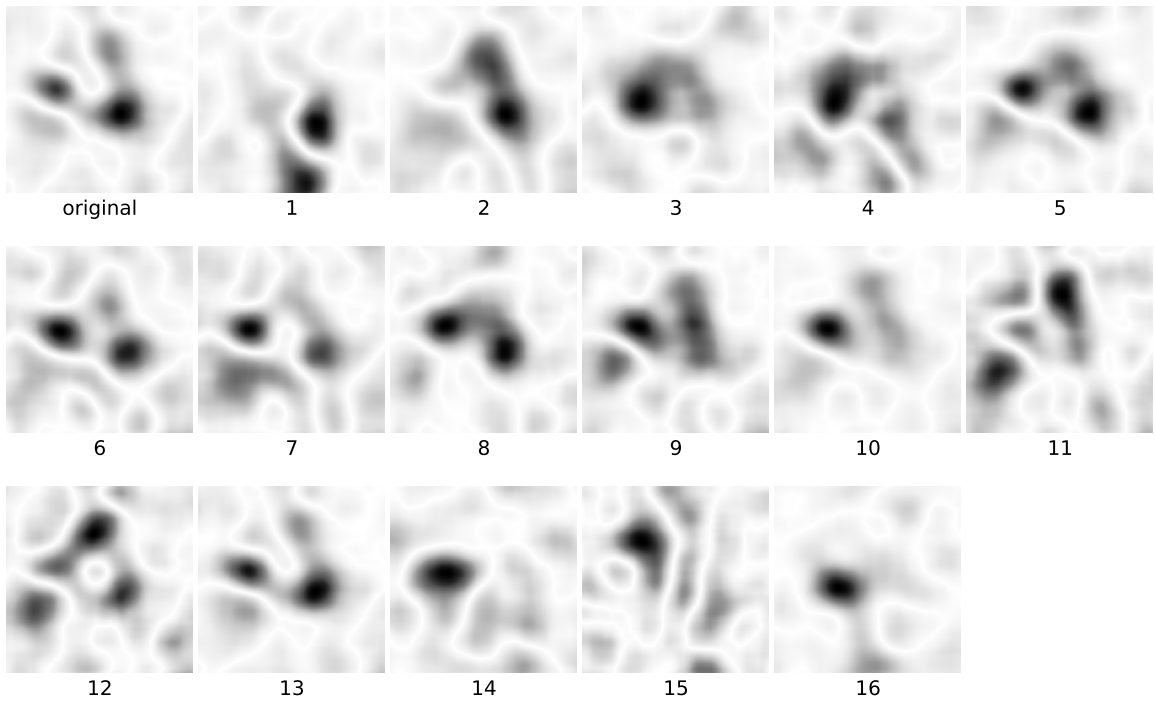


Figure 7: MPRT (independent) results. Like figure 5, except here for each image only one single layer has its weights perturbed while all other layers remain unchanged, starting with the final fully connected layer and ending with first layers of the model.

Layer	Top down	Bottom up	Independent
1	0.09	0.30	0.11
2	0.28	0.05	0.10
3	-0.10	0.22	0.11
4	0.02	-0.18	0.92
5	-0.24	-0.09	0.51
6	-0.11	0.17	0.38
7	-0.09	0.01	0.67
8	-0.04	-0.02	0.61
9	-0.11	0.02	0.32
10	-0.15	0.03	0.60
11	-0.13	-0.03	0.56
12	-0.19	0.02	0.63
13	-0.19	0.01	0.41
14	-0.21	-0.03	0.42
15	-0.27	-0.01	0.54
16	-0.22	0.02	0.18

Table 1: MPRT scores

4.3.1 HOW TO INTERPRET THESE RESULTS?

Consider these two hypothetical extremes:

1. The attribution map almost remains unchanged as a result of randomizing model layers. This happens when the explainer’s result is independent of the model. It is ignoring the model. Any patterns in the result are the explainer “doing the model’s work”. For instance, the explainer may do edge detection, which possibly is also what the model is expected to do. This would be undesired behavior for an explainer, because the explainer should strictly explain the model’s decisions without making assumptions itself about the data.
2. The attribution map changes completely after randomizing the first layer already, and keeps on changing for every additional randomized layer. This means the explainer’s result is highly dependent on the model, and does not indicate any hidden and invalid assumptions about the model. It is diserable behaviour for an explainer.

Overall, figures 5, 6 and 7 show results that demonstrate a strong dependency on the model and align well with the expected behavior of the explainer. In the top-down randomization of figure 5, progression in the randomization cascade is such that the information

is basically lost immediately after randomizing the first layer⁹, which is desirable as it indicates that the explainer’s output is highly dependent on the model’s learned parameters. This dependency ensures that the explainer is not generating results independently of the model but is instead accurately reflecting the model’s internal decision-making process. Note that randomization just shuffles the values within each layer. We need not worry about normalization issues.

The first independent randomized image in figure 7 should be the same (or at least similar) as the first bottom-up randomized image in figure 6. Indeed, we see approximately the same effect. The last three images in the independent run randomize the three fully connected layers of the VGG16 model. There we expect all remaining information to be destroyed and that is indeed what we see in these results. This is confirmed by what happens similarly in the first randomized image of the top-down order.

We do not fully understand in the independent order images why there are still so many images where the pattern looks almost the same as the original unperturbed one. How can it be that when any layer is completely randomized so much modelling information is preserved? Especially layers 5 through 13 look very much still like the unperturbed result. Another open question is why the first bottom-up and independent images are not exactly the same given equal random seeds. We leave these as open question for future research, because it is not the main focus of this work.

5 Qualitative assessment

In addition to the quantitative performance assessment done in Section 4, in this section we inspect results of experiments visually and describe our findings qualitatively. As well as thus providing our opinionated guide on how to interpret the attribution maps, this will cover aspects of performance that are overly complex to quantify. For instance, we will show that Nauta’s Consistency (Nauta et al., 2023) can be achieved in section 5.2.1. Contrastivity is tested by assessing the output of “Opposite” data items listed in section 3.2. Finally, Coherence is implicitly a main topic for almost all of this section.

5.1 Resulting attribution maps using default parameters

For those interested only in what in our opinion are the best possible results, we present first the attribution maps on all data item pairs defined in section 3.2 using the explainer with what we determined to be its default settings. These default settings are motivated in the following sections 5.2 and 5.3.

In figure 8 the image-versus-image model item pair attribution maps are displayed. The “bee versus fly” image highlights that the wings especially bring the bee’s image closer to that of a fly, while the stripes on the bee’s back drive it away from the fly. For the labradoodle, it seems like its eyes and its collar are especially labradoodle-like, which surprised us; a

9. Most “disruption” in the attribution map, caused by randomization of model layers, happens at the beginning, which indicates that the explainer performs well. Then progressive changes show weaker changes, which are expected if more layers are randomized.

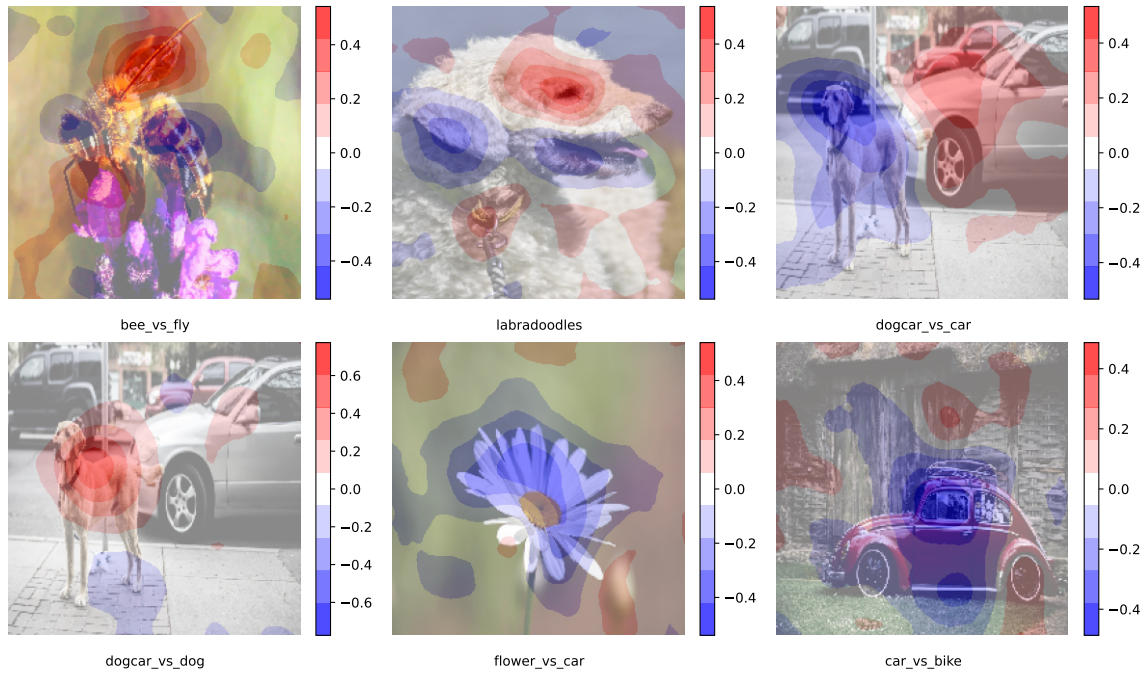


Figure 8: Attribution maps using default explainer parameter settings on the image-versus-image item pairs.

human would perhaps also identify its fur as distinctive. In the top right image, we compare the image containing both a dog and a car to a reference image of a car and indeed the car is highlighted as the distance-decreasing area, while the dog increases distance. As expected, the situation is reversed in the bottom left image in which the reference image contains another dog. In the bottom middle image, a flower is compared to a reference image of a car. While the algorithm detects that the flower moves the image away from the car region of embedded space, it does not find any regions that bring it closer to the car, which matches our expectation. Finally, the bottom right shows an image of a car compared to a reference image of a bicycle. Like the previous case, the car is highlighted as different from the reference, but the wheels are excluded from the strongly differing area. Indeed, bicycles have wheels in common with cars. The model does seem to distinguish somewhat between bicycle and car wheels, since the wheels are not indicated as a strong commonality. A human would perhaps conceptually group them together (as indeed the human authors of this work just did), but in terms of image classification, the correspondence is perhaps weaker.

Figure 9 shows the image-versus-caption model item pairs attribution maps. The first impression is that these attributions seem slightly less sharp in their delineations of the salient areas of interest. This might be an artifact of the model or of the fact that the parameters used in both cases may be less ideal for this model than for the image-versus-image cases. Nevertheless, the performance of the explainer on this model, too, is convincing.

5.2 Parameter exploration

While we strove to minimize the number of free parameters of the algorithm, we could not eliminate them all. For the remaining parameters, we found default values that give decent results for the experiments in this paper, as shown in the galleries in the previous section. However, in different situations (e.g. a different model, data sizes, data modalities, or even different objects of interest within the data items), the optimal parameters must be tuned. In this section, we explore the effects of non-default parameter choices in case of our own model and data choices. This can serve as a starting point for optimal tuning of our algorithm on experiments beyond those in this work.

5.2.1 NUMBER OF MASKS

The higher the number of masks used, the more stable the attribution map becomes, as more samples are being used to average over as part of the algorithm. The statistics of this are shown in table 2. With increasing number of masks, the difference decreases between maps produced with a different set of random masks. The true attribution pattern reveals itself through a decrease in the mean pixel standard deviation. A visual inspection of figure 10, where we show attribution maps obtained by running the explainer using different initial random-generator-seeds, yields the same conclusion. The patterns become increasingly similar with increasing number of masks.

EXPLAINABLE EMBEDDINGS WITH DISTANCE EXPLAINER

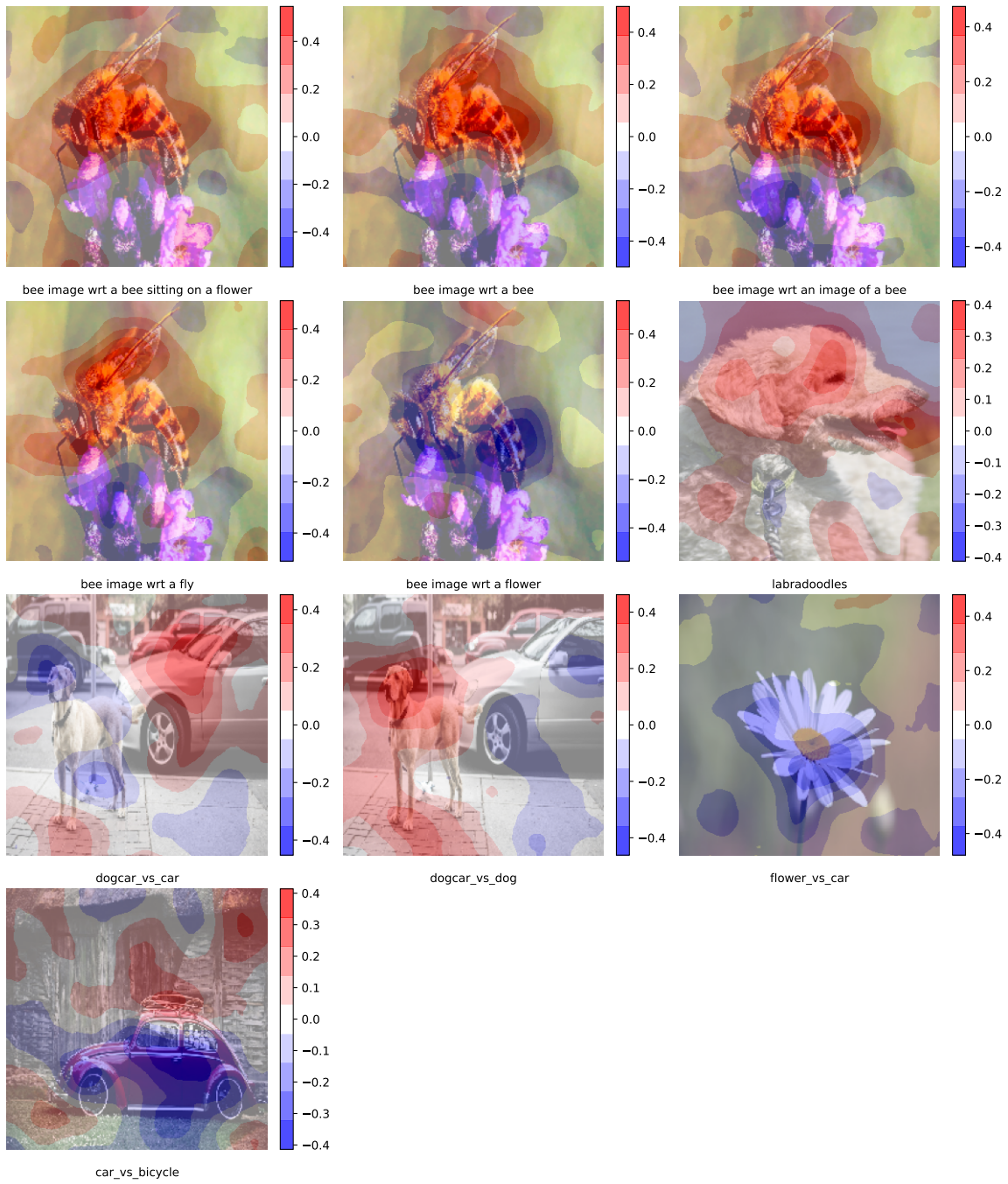


Figure 9: Attribution maps using default explainer parameter settings on the image-versus-caption item pairs.

Number of masks	Mean STD per pixel		
	bee vs fly	flower vs car	dogcar vs car
100	0.139	0.140	0.140
500	0.064	0.062	0.062
2000	0.031	0.031	0.032

Table 2: Statistics showing how an increase in number of masks decreases standard deviation between maps produced with a different initial random seed. The three columns show that this happens regardless of the exact data pairs.

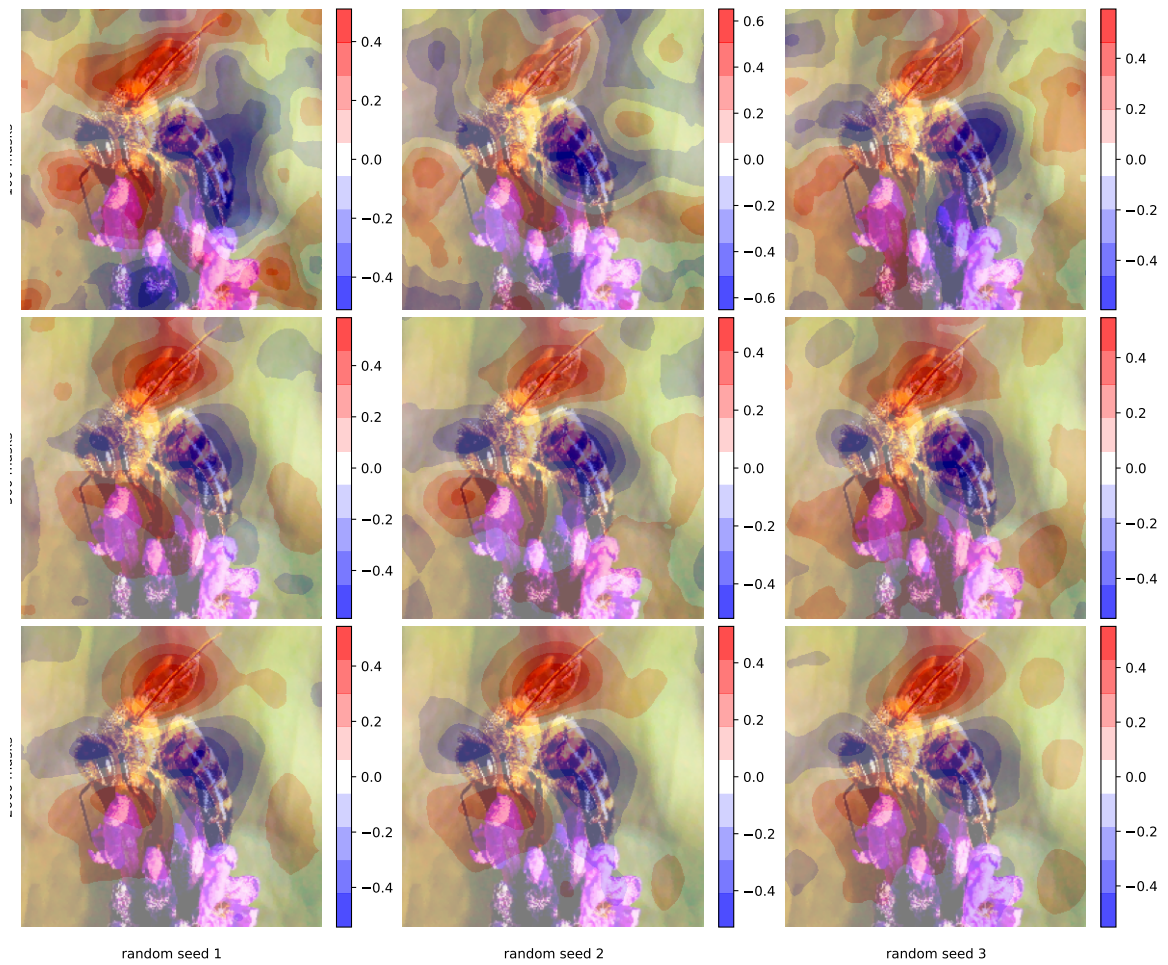
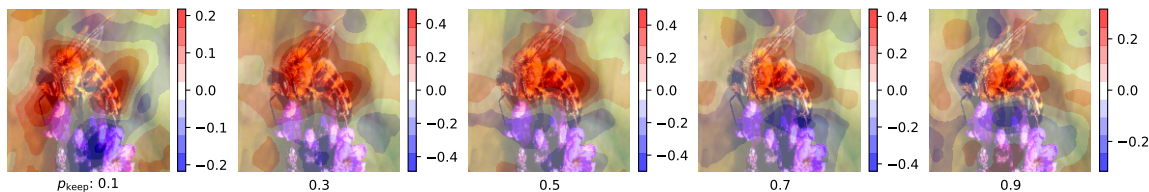


Figure 10: Convergence of the attribution map with increasing number of masks (rows) shown for three different random seeds (columns) for the case of comparing the bee image to the fly image.

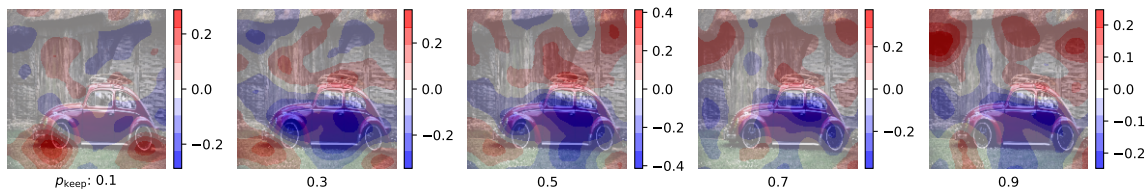
As noted before, the numbers in table 2 do not generalize to all use-cases of Distance Explainer. Different resolution images, particular embedding models, etcetera, will require fine-tuning of the number of masks. Also changing other Distance Explainer parameters may necessitate re-tuning the number of masks, as we discuss in section 5.2.3. For the purpose of this work, unless otherwise noted, we use 1000 masks. We confirmed that in these cases 1000 masks provides a decent trade-off between stability/accuracy, computational cost and experimental complexity.¹⁰

5.2.2 MASK COVERAGE PERCENTAGE

The proportion of pixels to keep unmasked in each random mask, p_{keep} , plays a subtle role. What value for p_{keep} results in the most informative output, is dependent on the specific data item and the particular salient features. We found two cases that illustrate this.



(a) Image of a bee versus caption “a bee”.



(b) Image of a car versus caption “a bicycle”.

Figure 11: From left to right, p_{keep} is increased, showing values: 0.1, 0.3, 0.5, 0.7, 0.9.

The first case is again that of the image of the bee, using the image-versus-caption model to determine its distance to various captions like “a bee”, “a flower”, “a fly” or the more explicit “an image of a bee”. The explainer in these cases works best at values around the center of the p_{keep} range, i.e. roughly between 0.4 and 0.6, and decreases in performance

10. We should note that there were other cases – not shown in this work – where we only saw stabilization around 5000 masks. For instance, one case was of an image containing both two partially obscured cars and one fully shown dog compared to the caption “a dog”. In this case, while the large scale features (the dog and the cars) stabilized at 1000 masks, a negative highlight (i.e. a “distance increasing” attribution area) started stabilizing on one of the wheels at the higher number of masks only. If users are interested in certain details, they should hence explore the optimal number of masks for their use-case.

Another test case we explored was to compare an image of a flower to the caption query “a car”, i.e. to compare two completely orthogonal embedded vectors. In this case, again, the attribution map only stabilized at 5000 masks, although at less masks it seemed more or less usable. There was more noise around the flower at 1000 and 2000 masks. Whether this is relevant will differ per use-case.

the further one sets p_{keep} towards 0 or 1. A decrease in performance in these cases mainly means noisy spots appearing, i.e. patches of high attribution values that do not reflect any salient parts of the image. The average amplitude of the attribution map also tends to decrease towards p_{keep} of 0 or 1, which also increases the relative amplitude of possibly already lingering noisy patches, thus increasing the appearance of noise. This is illustrated in figure 11a.

The second case is that of an image of a car compared to the caption “a bicycle”, as shown in figure 11b. In this case, we found that there are two interesting p_{keep} ranges that explain different parts of the image. At values between 0.01 and 0.1 the car’s wheels are highlighted. At these low masking values, this is indeed something you could expect; if for some masks only the wheels are left in the image, the model might think it’s (part of) a bicycle. Mostly the bottom of the wheels are highlighted, so it seems to interpret the car fenders as proof against this being an image of a bicycle, which also makes sense. At 0.3 this tendency has faded away completely. Values between 0.2 and 0.9 highlight the car body, with other parts of the images remaining quite spotty. It’s hard in this case to say what is an optimal value of p_{keep} . Two different patterns emerge in two different ranges. Only 0.2 seems to cover both patterns, but sub-optimally. The range of 0.05-0.1 seems optimal for the wheels, while 0.2-0.7 are fine for the car body (with again a preference towards the central values around 0.5, where the average amplitude is higher and noise lower).

These cases illustrate that the particulars of the data items play an important role in the performance of the explainer under different parameter settings. We recommend users of the algorithm to do a sweep of this parameter. Possibly, a multi-parameter combination of attribution maps could be made, but we leave this as a topic of future study.

5.2.3 MASK FEATURE RESOLUTION

In figure 12 we illustrate the effect of changing the number of random “superpixel” areas to split the random masking into. The numbers below each panel indicate the feature resolution: the number of features along both image axes. We see that resolutions of 2 and 4 are too coarse for this image. Everything above 32 is also useless, but for a different reason: it becomes too noisy. This can be compensated by using more masks. It makes sense that when trying to differentiate one class from a similar other class, that details of the input need to be taken into account and therefore a higher feature resolution is necessary. At values of 8 to 16 we see that the salient parts of the bee, like its wings, are more precisely delineated. So, also for this parameter, the perfect number of features depends on the purpose of the explanation (which determines the scale) and a cost-benefit analysis, because finer resolution requires more masks.

We ran a follow-up experiment with more masks to confirm that the noise would disappear as we expected. We indeed see that the noise disappears as we increase the number of used masks as illustrated in figure 13. We do see that for image-versus-caption cases, even more masks are needed to reach the same level of noise reduction as for the image-versus-image case. This matches our earlier observation of figure 9 in section 5.1.

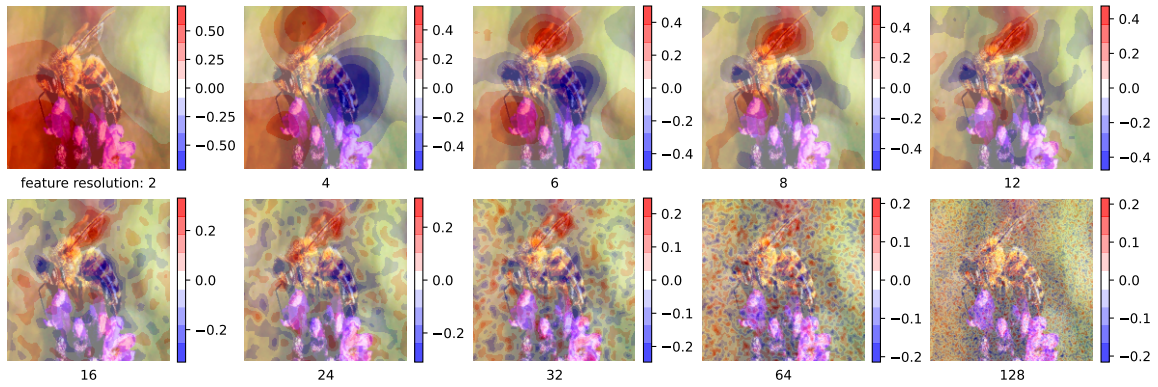


Figure 12: The effect of using different mask feature resolution is shown. The number of features in both image axis directions is shown below each panel.

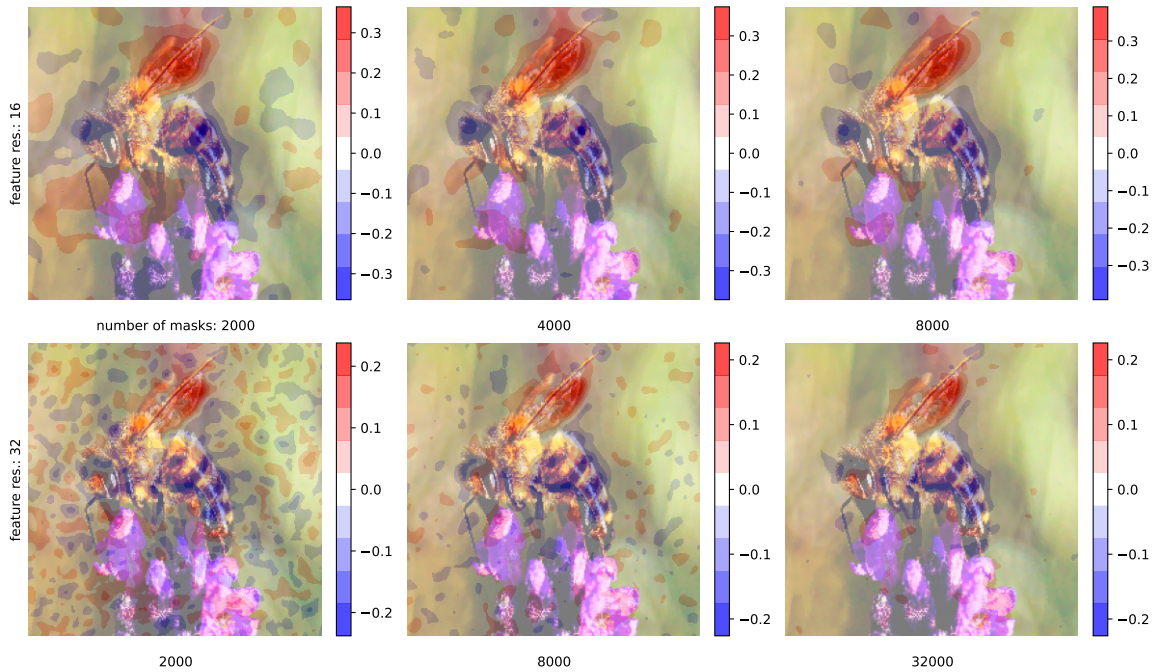


Figure 13: The effect of increasing the number of masks on different mask feature resolution results are shown. Each row represents a different feature resolution, with the number of masks used shown below each panel.

5.3 Mask selection

As explained in section 2, we replaced the RISE algorithm’s mask *weighting* with a mask *selection* step. There are multiple ways to select the masks which we explore in this section.

5.3.1 ONE-SIDED VS TWO-SIDED

We first explore the effect of using one-sided versus two-sided mask selection. In the one-sided case, we only select the top n -percent masks, i.e. those that decrease the distance to the reference point. In the two-sided case, we select both the top n -percent masks and the bottom n -percent masks, i.e. those that increase the distance to the reference point. We multiply the bottom n -percent masked attribution maps by -1 before adding them to the rest.

We ran the explainer on the Resnet50 model and the “bee versus fly” case using the top n -percent masks and compared the attribution maps with the same run while using the bottom n -percent masks, showing the results in figure 14. We conclude that both cases yield an almost indistinguishable pattern, and are both measuring a similar signal. This led us to conclude that the two-sided approach is the better one, as it allows us to use all masks and therefore more data, averaging out noise in the final attribution map.

Looking at the columns of figure 14, we see that across the range of mask selection percentages, from 10 to 50%, the signal remains more or less stable. This suggests that either most of the signal amplitude is contained in the first 10% of the masks, or all mask ranges contain similar information but also similar noise. We will look at this in more detail in section 5.3.3.

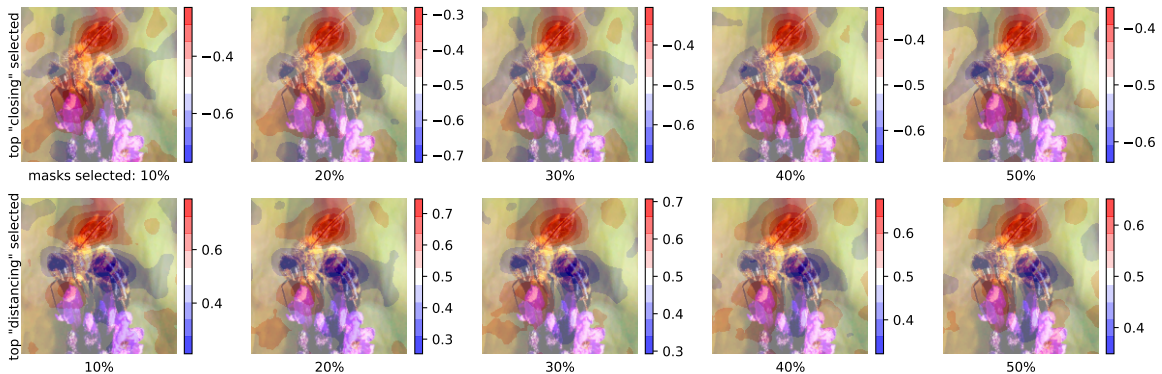


Figure 14: Attribution maps produced using one-sided mask selection. Explaining the Resnet50 model on the “bee versus fly” case. Top row: only selecting from the top distance-decreasing masks. Bottom row: only selecting from the top distance-increasing masks (multiplied by -1 for easier comparison). From left to right, the percentage of selected masks is increased.

5.3.2 THRESHOLD VALUE

Having chosen the two-sided “mirror” approach, we next studied the effect in this mode on the selection range of distance rank-ordered masks. Figure 15 shows how an increase in the selection thresholds (i.e. increasing inclusion of data) does not produce any meaningful changes in the attribution map patterns beyond a threshold of 10%. Neither the highlighted regions change significantly, nor does the quality of the maps (i.e. there is no major change in noise patterns). One could expect some discreteness effects with less data, but we see none for the thresholds we use. Concluding from this, we set our default threshold value to 10%.

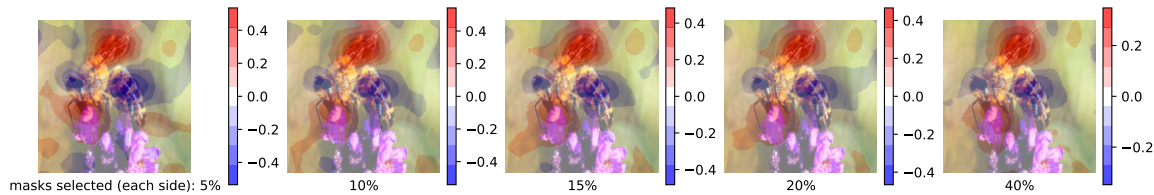


Figure 15: Attribution maps produced using two-sided “mirror” mask selection. Explaining the Resnet50 model on the “bee versus fly” case. From left to right, the percentage of selected masks is increased.

5.3.3 NON-SELECTED MASKS

Finally, for completeness’ sake, we ask what information is in the masks that were discarded by our selection filter(s). In figure 16, we compare an attribution map of the two-sided 10% setting we motivated in the above two sections, to four maps generated by combining slices of the discarded percentage ranges of the masks.

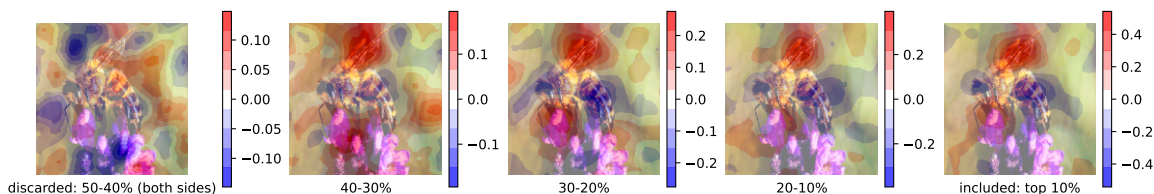


Figure 16: Image vs image: bee versus fly. The panels show attribution maps from two-sided masking threshold range slices indicated below the panels. The left four panels show results from masks that are **excluded** from the usual attribution maps. The right panel for comparison shows a default settings attribution map (i.e. the result from masks that **are** included).

The first map, composed of the masks in the center of the ranking order, barely contains any signal at all. In the other three discarded maps one can start discerning the expected patterns, but they still contain more noise and therefore result in a less clear map. The

noise decreases towards the higher end of the ranking order. We conclude that masks that are closer to the top and bottom sections have a higher signal to noise ratio.

6 Discussion

The proposed method provides a novel approach to explaining distances in embedded spaces, building on the principles of saliency-based attribution. Our experiments demonstrate that the method effectively identifies features contributing to the similarity or dissimilarity between embedded data points. While the primary focus in this paper has been on image-based embeddings, the methodology is flexible and can be easily extended to other modalities, such as text and multi-modal embeddings. One such multi-modal application we demonstrated in this paper; we performed all our experiments on the image-versus-caption model as well and found comparable end-results to those in the image-versus-image experiments.

One of the key challenges we encountered is parameter tuning, particularly in selecting the appropriate number of masks and filtering criteria. The method’s reliance on random masking introduces a trade-off between computational cost and stability of results. Additionally, we expect that different embedding models may require tailored distance metrics to better capture the underlying structure of their embedded spaces.

Moreover, alternative perturbation strategies could be explored to reduce the risk of generating out-of-distribution inputs that might affect model behavior. In particular, the imputation method of RISE is simplistic and results in possible out-of-distribution inputs for the model. In this work, we left this imputation method unchanged and used it for our own algorithm.

Another consideration is the interpretability of the resulting attribution maps. While they provide meaningful insights for AI researchers and developers, their utility for non-expert users remains an open question. Future work could explore user studies to assess the comprehensibility of explanations across different audiences. In particular, we are interested in how academic researchers can leverage this tool to improve their AI-enhanced research.

7 Conclusion

We introduced a method to explain distances in embedded spaces using a saliency-based approach adapted from RISE. By analyzing the impact of input perturbations on similarity metrics, our method generates local explanations that highlight which features contribute most to embedding proximity or separation.

Our experimental results demonstrate the efficacy of this approach across a small number of different models and data modalities, particularly in image-based and multi-modal embeddings. Quantitative evaluations confirm that our method maintains robustness, consistency, and dependency on model parameters, aligning with established XAI evaluation criteria.

Future work could focus on refining the method for text and other non-visual embeddings, exploring alternative distance metrics, and optimizing and possibly automating pa-

parameter selection. Additionally, studies on the human interpretability of these explanations could provide insights into their usability in real-world applications.

Acknowledgements

We want to thank Willem van der Spek for fruitful discussions and feedback on our quantitative evaluation and for providing an implementation for Incremental Deletion. We also thank Jisk Attema and Elena Rangelova for helpful discussions about the algorithm and the experimental setup.

Research software usage

Software used in our Distance Explainer algorithm includes: DIANNA (Rangelova et al., 2024), NumPy (Harris et al., 2020), scikit-learn (Pedregosa et al., 2011), tqdm, pyyaml and dataclass_wizard. For the analysis in this paper, we additionally used Matplotlib (Hunter, 2007), Quantus (Hedström et al., 2023), Keras (Chollet et al., 2015), PyTorch (Ansel et al., 2024), torchtext, CLIP (Radford et al., 2021), gitpython and Pillow.

Generative AI assistance

We used ChatGPT 4o on 21 Jan 2025 for refining the Discussion and Conclusion texts, used NotebookLM on 28 Jan 2025 to refine our introduction text, again ChatGPT 4o through Copilot on 11, 24 and 25 April 2025 for refining sections 4 and 5 and Claude 3.7 Sonnet and Mistral on 6 May 2025 to refine section 4. The abstract was written using Claude 3.7 Sonnet and NotebookLM on 20 May 2025. All AI-output has been verified for correctness, accuracy and completeness, adapted where needed, and approved by the authors.

References

- Reduan Achtibat, Maximilian Dreyer, Ilona Eisenbraun, Sebastian Bosse, Thomas Wiegand, Wojciech Samek, and Sebastian Lapuschkin. From attribution maps to human-understandable explanations through concept relevance propagation. *Nature Machine Intelligence*, 5(9):1006–1019, 9 2023. ISSN 2522-5839. doi: 10.1038/s42256-023-00711-8. URL <https://doi.org/10.1038/s42256-023-00711-8>.
- Julius Adebayo, Justin Gilmer, Michael Muelly, Ian Goodfellow, Moritz Hardt, and Been Kim. Sanity checks for saliency maps, 2020. URL <https://arxiv.org/abs/1810.03292>.
- Sajid Ali, Tamer Abuhmed, Shaker El-Sappagh, Khan Muhammad, Jose M. Alonso-Moral, Roberto Confalonieri, Riccardo Guidotti, Javier Del Ser, Natalia Díaz-Rodríguez, and Francisco Herrera. Explainable artificial intelligence (xai): What we know and what is left to attain trustworthy artificial intelligence. *Inf. Fusion*, 99(C), November 2023. ISSN 1566-2535. doi: 10.1016/j.inffus.2023.101805. URL <https://doi.org/10.1016/j.inffus.2023.101805>.

- Jason Ansel, Edward Yang, Horace He, Natalia Gimelshein, Animesh Jain, Michael Voznesensky, Bin Bao, Peter Bell, David Berard, Evgeni Burovski, Geeta Chauhan, Anjali Chourdia, Will Constable, Alban Desmaison, Zachary DeVito, Elias Ellison, Will Feng, Jiong Gong, Michael Gschwind, Brian Hirsh, Sherlock Huang, Kshiteej Kalambarkar, Laurent Kirsch, Michael Lazos, Mario Lezcano, Yanbo Liang, Jason Liang, Yinghai Lu, CK Luk, Bert Maher, Yunjie Pan, Christian Puhersch, Matthias Reso, Mark Saroufim, Marcos Yukio Siraichi, Helen Suk, Michael Suo, Phil Tillet, Eikan Wang, Xiaodong Wang, William Wen, Shunting Zhang, Xu Zhao, Keren Zhou, Richard Zou, Ajit Mathews, Gregory Chanan, Peng Wu, and Soumith Chintala. PyTorch 2: Faster Machine Learning Through Dynamic Python Bytecode Transformation and Graph Compilation. In *29th ACM International Conference on Architectural Support for Programming Languages and Operating Systems, Volume 2 (ASPLOS '24)*. ACM, April 2024. doi: 10.1145/3620665.3640366. URL <https://pytorch.org/assets/pytorch2-2.pdf>.
- David Bau, Jun-Yan Zhu, Hendrik Strobelt, Agata Lapedriza, Bolei Zhou, and Antonio Torralba. Understanding the role of individual units in a deep neural network. *Proceedings of the National Academy of Sciences*, 117(48):30071–30078, 2020. doi: 10.1073/pnas.1907375117. URL <https://www.pnas.org/doi/abs/10.1073/pnas.1907375117>.
- Umang Bhatt, Adrian Weller, and José M. F. Moura. Evaluating and aggregating feature-based model explanations. In *Proceedings of the Twenty-Ninth International Joint Conference on Artificial Intelligence, IJCAI'20*, 2021. ISBN 9780999241165.
- Roberto Boselli, Simone D’Amico, and Navid Nobani. explainable ai for word embeddings: A survey. *Cognitive Computation*, 17(1):19, 12 2024. ISSN 1866-9964. doi: 10.1007/s12559-024-10373-2. URL <https://doi.org/10.1007/s12559-024-10373-2>.
- François Chollet et al. Keras. <https://keras.io>, 2015.
- Grzegorz Chrupala. Visually grounded models of spoken language - a survey of datasets, architectures and evaluation techniques. *Journal of Artificial Intelligence Research*, 73: 673–707, February 2022. doi: 10.1613/jair.1.12967. DBLP’s bibliographic metadata records provided through <http://dblp.org/search/publ/api> are distributed under a Creative Commons CC0 1.0 Universal Public Domain Dedication. Although the bibliographic metadata records are provided consistent with CC0 1.0 Dedication, the content described by the metadata records is not. Content may be subject to copyright, rights of privacy, rights of publicity and other restrictions. Publisher Copyright: © 2022 AI Access Foundation. All rights reserved.
- Kenneth Ward Church. Word2vec. *Natural Language Engineering*, 23(1):155–162, 2017. doi: 10.1017/S1351324916000334.
- Alexey Dosovitskiy, Lucas Beyer, Alexander Kolesnikov, Dirk Weissenborn, Xiaohua Zhai, Thomas Unterthiner, Mostafa Dehghani, Matthias Minderer, Georg Heigold, Sylvain

- Gelly, Jakob Uszkoreit, and Neil Houlsby. An image is worth 16x16 words: Transformers for image recognition at scale, 2021. URL <https://arxiv.org/abs/2010.11929>.
- Krishna Gade, Sahin Cem Geyik, Krishnaram Kenthapadi, Varun Mithal, and Ankur Taly. Explainable ai in industry. In *Proceedings of the 25th ACM SIGKDD International Conference on Knowledge Discovery & Data Mining, KDD '19*, page 3203–3204, New York, NY, USA, 2019. Association for Computing Machinery. ISBN 9781450362016. doi: 10.1145/3292500.3332281. URL <https://doi.org/10.1145/3292500.3332281>.
- Caroline M. Gevaert. Explainable ai for earth observation: A review including societal and regulatory perspectives. *International Journal of Applied Earth Observation and Geoinformation*, 112:102869, 2022. ISSN 1569-8432. doi: <https://doi.org/10.1016/j.jag.2022.102869>. URL <https://www.sciencedirect.com/science/article/pii/S1569843222000711>.
- Charles R. Harris, K. Jarrod Millman, Stéfan J. van der Walt, Ralf Gommers, Pauli Virtanen, David Cournapeau, Eric Wieser, Julian Taylor, Sebastian Berg, Nathaniel J. Smith, Robert Kern, Matti Picus, Stephan Hoyer, Marten H. van Kerkwijk, Matthew Brett, Allan Haldane, Jaime Fernández del Río, Mark Wiebe, Pearu Peterson, Pierre Gérard-Marchant, Kevin Sheppard, Tyler Reddy, Warren Weckesser, Hameer Abbasi, Christoph Gohlke, and Travis E. Oliphant. Array programming with NumPy. *Nature*, 585(7825):357–362, September 2020. doi: 10.1038/s41586-020-2649-2. URL <https://doi.org/10.1038/s41586-020-2649-2>.
- Anna Hedström, Leander Weber, Daniel Krakowczyk, Dilyara Bareeva, Franz Motzkus, Wojciech Samek, Sebastian Lapuschkin, and Marina M.-C. Höhne. Quantus: An explainable ai toolkit for responsible evaluation of neural network explanations and beyond. *Journal of Machine Learning Research*, 24(34):1–11, 2023. URL <http://jmlr.org/papers/v24/22-0142.html>.
- Anna Hedström, Leander Weber, Sebastian Lapuschkin, and Marina MC Höhne. Sanity checks revisited: An exploration to repair the model parameter randomisation test, 2024. URL <https://arxiv.org/abs/2401.06465>.
- Florian Huber, Lars Ridder, Stefan Verhoeven, Jurriaan H. Spaaks, Faruk Diblen, Simon Rogers, and Justin J. J. van der Hooft. Spec2vec: Improved mass spectral similarity scoring through learning of structural relationships. *PLOS Computational Biology*, 17(2):1–18, 02 2021. doi: 10.1371/journal.pcbi.1008724. URL <https://doi.org/10.1371/journal.pcbi.1008724>.
- J. D. Hunter. Matplotlib: A 2d graphics environment. *Computing in Science & Engineering*, 9(3):90–95, 2007. doi: 10.1109/MCSE.2007.55.
- Diederik P. Kingma and Max Welling. An introduction to variational autoencoders. *Foundations and Trends® in Machine Learning*, 12(4):307–392, 2019. ISSN 1935-8245. doi: 10.1561/22000000056. URL <http://dx.doi.org/10.1561/22000000056>.

- Christiaan Meijer. Masking time-series for explainable ai. <https://blog.esciencecenter.nl/masking-time-series-for-explainable-ai-90247ac252b4>, 2024. Accessed: 18 October 2024.
- Meike Nauta, Jan Trienes, Shreyasi Pathak, Elisa Nguyen, Michelle Peters, Yasmin Schmitt, Jörg Schlötterer, Maurice van Keulen, and Christin Seifert. From anecdotal evidence to quantitative evaluation methods: A systematic review on evaluating explainable ai. *ACM Comput. Surv.*, 55(13s), 7 2023. ISSN 0360-0300. doi: 10.1145/3583558. URL <https://doi.org/10.1145/3583558>.
- F. Pedregosa, G. Varoquaux, A. Gramfort, V. Michel, B. Thirion, O. Grisel, M. Blondel, P. Prettenhofer, R. Weiss, V. Dubourg, J. Vanderplas, A. Passos, D. Cournapeau, M. Brucher, M. Perrot, and E. Duchesnay. Scikit-learn: Machine learning in Python. *Journal of Machine Learning Research*, 12:2825–2830, 2011.
- Vitali Petsiuk, Abir Das, and Kate Saenko. Rise: Randomized input sampling for explanation of black-box models, 2018. URL <https://arxiv.org/abs/1806.07421>.
- Alec Radford, Jong Wook Kim, Chris Hallacy, Aditya Ramesh, Gabriel Goh, Sandhini Agarwal, Girish Sastry, Amanda Askell, Pamela Mishkin, Jack Clark, Gretchen Krueger, and Ilya Sutskever. Learning transferable visual models from natural language supervision, 2021. URL <https://arxiv.org/abs/2103.00020>.
- Elena Rangelova, Patrick Bos, Yang Liu, Christiaan Meijer, Fakhreh (Sarah) Alidoost, Leon Oostrum, Giulia Crocioni, Aron Jansen, Laura Ootes, Pranav Chandramouli, Stef Smeets, and Willem van der Spek. dianna, October 2024. URL <https://doi.org/10.5281/zenodo.14337052>.
- Marco Ribeiro, Sameer Singh, and Carlos Guestrin. “why should I trust you?”: Explaining the predictions of any classifier. In John DeNero, Mark Finlayson, and Sravana Reddy, editors, *Proceedings of the 2016 Conference of the North American Chapter of the Association for Computational Linguistics: Demonstrations*, pages 97–101, San Diego, California, June 2016. Association for Computational Linguistics. doi: 10.18653/v1/N16-3020. URL <https://aclanthology.org/N16-3020>.
- Germans Savcisens, Tina Eliassi-Rad, Lars Kai Hansen, Laust Hvas Mortensen, Lau Lilleholt, Anna Rogers, Ingo Zettler, and Sune Lehmann. Using sequences of life-events to predict human lives. *Nature Computational Science*, 4(1):43–56, 1 2024. ISSN 2662-8457. doi: 10.1038/s43588-023-00573-5. URL <https://doi.org/10.1038/s43588-023-00573-5>.
- Florian Schroff, Dmitry Kalenichenko, and James Philbin. Facenet: A unified embedding for face recognition and clustering. In *2015 IEEE Conference on Computer Vision and Pattern Recognition (CVPR)*, pages 815–823. IEEE, June 2015. doi: 10.1109/cvpr.2015.7298682. URL <http://dx.doi.org/10.1109/CVPR.2015.7298682>.

- Ramprasaath R. Selvaraju, Michael Cogswell, Abhishek Das, Ramakrishna Vedantam, Devi Parikh, and Dhruv Batra. Grad-cam: Visual explanations from deep networks via gradient-based localization. *Int. J. Comput. Vision*, 128(2):336–359, 2 2020. ISSN 0920-5691. doi: 10.1007/s11263-019-01228-7. URL <https://doi.org/10.1007/s11263-019-01228-7>.
- Atefeh Shahroudjed. A survey on understanding, visualizations, and explanation of deep neural networks, 2021. URL <https://arxiv.org/abs/2102.01792>.
- Willem van der Spek. Explaining the explainer. Master’s thesis, University of Amsterdam (UvA), Amsterdam, Netherlands, 9 2023. Available at https://staff.fnwi.uva.nl/a.s.z.belloum/MSctheses/MScthesis_Willem_van_der_Spec.pdf.
- Giulia Vilone and Luca Longo. Classification of explainable artificial intelligence methods through their output formats. *Machine Learning and Knowledge Extraction*, 3(3):615–661, 2021. ISSN 2504-4990. doi: 10.3390/make3030032. URL <https://www.mdpi.com/2504-4990/3/3/32>.
- Guang Yang, Qinghao Ye, and Jun Xia. Unbox the black-box for the medical explainable ai via multi-modal and multi-centre data fusion: A mini-review, two showcases and beyond. *Information Fusion*, 77:29–52, 2022. ISSN 1566-2535. doi: <https://doi.org/10.1016/j.inffus.2021.07.016>. URL <https://www.sciencedirect.com/science/article/pii/S1566253521001597>.
- Chih-Kuan Yeh, Cheng-Yu Hsieh, Arun Sai Suggala, David I. Inouye, and Pradeep Ravikumar. On the (in)fidelity and sensitivity of explanations. In *Proceedings of the 33rd International Conference on Neural Information Processing Systems*, Red Hook, NY, USA, 2019. Curran Associates Inc.